



Modeling the Growth of Aluminum Gallium Nitride ((Al)GaN) Films Grown on Aluminum Nitride (AlN) Substrates

**by Dr. Kenneth A. Jones, Dr. Anthony J. Ciani, Dr. Iskander Batyrev,
and Dr. Peter W. Chung**

ARL-MR-0770

March 2011

NOTICES

Disclaimers

The findings in this report are not to be construed as an official Department of the Army position unless so designated by other authorized documents.

Citation of manufacturer's or trade names does not constitute an official endorsement or approval of the use thereof.

Destroy this report when it is no longer needed. Do not return it to the originator.

Army Research Laboratory

Adelphi, MD 20783-1197

ARL-MR-0770**March 2011**

Modeling the Growth of Aluminum Gallium Nitride ((Al)GaN) Films Grown on Aluminum Nitride (AlN) Substrates

Dr. Kenneth A. Jones

Sensors and Electron Devices Directorate, ARL

Dr. Anthony J. Ciani

Computational and Information Sciences Directorate, ARL

Dr. Iskander Batyrev

Weapons and Materials Research Directorate, ARL

and

Dr. Peter W. Chung

Computational and Information Sciences Directorate, ARL

REPORT DOCUMENTATION PAGE				Form Approved OMB No. 0704-0188	
<p>Public reporting burden for this collection of information is estimated to average 1 hour per response, including the time for reviewing instructions, searching existing data sources, gathering and maintaining the data needed, and completing and reviewing the collection information. Send comments regarding this burden estimate or any other aspect of this collection of information, including suggestions for reducing the burden, to Department of Defense, Washington Headquarters Services, Directorate for Information Operations and Reports (0704-0188), 1215 Jefferson Davis Highway, Suite 1204, Arlington, VA 22202-4302. Respondents should be aware that notwithstanding any other provision of law, no person shall be subject to any penalty for failing to comply with a collection of information if it does not display a currently valid OMB control number.</p> <p>PLEASE DO NOT RETURN YOUR FORM TO THE ABOVE ADDRESS.</p>					
1. REPORT DATE (DD-MM-YYYY) March 2011		2. REPORT TYPE DRI		3. DATES COVERED (From - To) October 2009 to September 2010	
4. TITLE AND SUBTITLE Modeling the Growth of Aluminum Gallium Nitride ((Al)GaN) Films Grown on Aluminum Nitride (AlN) Substrates				5a. CONTRACT NUMBER	
				5b. GRANT NUMBER	
				5c. PROGRAM ELEMENT NUMBER	
6. AUTHOR(S) Dr. Kenneth A. Jones, Dr. Anthony J. Ciani, Dr. Iskander Batyrev, and Dr. Peter W. Chung				5d. PROJECT NUMBER	
				5e. TASK NUMBER	
				5f. WORK UNIT NUMBER	
7. PERFORMING ORGANIZATION NAME(S) AND ADDRESS(ES) U.S. Army Research Laboratory ATTN: RDRL-SED-E 2800 Powder Mill Road Adelphi, MD 20783-1197				8. PERFORMING ORGANIZATION REPORT NUMBER ARL-MR-0770	
9. SPONSORING/MONITORING AGENCY NAME(S) AND ADDRESS(ES)				10. SPONSOR/MONITOR'S ACRONYM(S)	
				11. SPONSOR/MONITOR'S REPORT NUMBER(S)	
12. DISTRIBUTION/AVAILABILITY STATEMENT Approved for public release; distribution unlimited.					
13. SUPPLEMENTARY NOTES					
14. ABSTRACT <p>The goal of this research was to determine if the evolution of dislocations in aluminum gallium nitride (AlGaN) films grown on aluminum nitride (AlN) substrates could be modeled with the goal of determining if there are conditions under which the films are grown so that most of the dislocations created by the mismatch are confined to regions away from the film surface where devices are fabricated. Through crystallographic modeling, we determined that the most probable slip system is the $(11\bar{2}2)^{1/3}\langle 11\bar{2}3 \rangle$ secondary slip system. We also calculated that the energy states associated with the dislocations lie in or near the energy bands, but that the stacking faults create deep donors that can compensate p-type dopants. Modifications to the Parallel Dislocation Simulator (ParaDIS) code used to calculate dislocation creation in face centered cubic (FCC) metals under stress were begun to adapt it for wurtzite hexagonal close packed (HCP) semiconductors such as AlGaN. This includes changing from the 3-Miller indices system used for FCC structures to the 4-Miller indices systems used for HCP structures. The next step is to apply our modified model to the selected slip system.</p>					
15. SUBJECT TERMS Gallium nitride, aluminum nitride, modeling, semiconductor film growth					
16. SECURITY CLASSIFICATION OF:			17. LIMITATION OF ABSTRACT UU	18. NUMBER OF PAGES 26	19a. NAME OF RESPONSIBLE PERSON Dr. Kenneth A. Jones
a. REPORT Unclassified	b. ABSTRACT Unclassified	c. THIS PAGE Unclassified			19b. TELEPHONE NUMBER (Include area code) (301) 394-2005

Contents

List of Figures	iv
List of Tables	iv
1. Objective	1
2. Approach	1
3. Results	2
3.1 Slip Systems Analysis	2
3.2 Simulations of Dislocation Motion	10
3.3 Modeling the Defects	12
4. Conclusions	14
5. References	16
6. Transitions	17
List of Symbols, Abbreviations, and Acronyms	18
Distribution List	20

List of Figures

Figure 1. (a) Schematic of a dislocation loop composed of a 60° $(111)/\frac{1}{2}[01\bar{1}]$ and a $\frac{1}{2}[01\bar{1}]$ screw dislocation created at the surface to relieve the mismatch strain. (b) Formation of a third 60° $(111)/\frac{1}{2}[01\bar{1}]$ mismatch dislocation, and all of the associated partials. (c) Schematic of a 60° $(111)/\frac{1}{2}[01\bar{1}]$ dislocation and (d) its decomposition into $\frac{1}{6}[11\bar{2}]$ and $\frac{1}{6}[\bar{1}21]$ partial dislocations.	3
Figure 2. Schematic of the (a) $(01\bar{1}1)/\frac{1}{3}[\bar{1}12\bar{3}]$ and (b) $(11\bar{2}2)/\frac{1}{3}[\bar{1}12\bar{3}]$ slip systems in hexagonal materials.	5
Figure 3. (a) Geometric description of the stacking of the close packed planes in zinc blende and wurtzite crystals, and the $[\bar{1}2\bar{1}]$ or $[01\bar{1}0]$ trace formed by the intersection of the $(20\bar{2})$ or $(2\bar{1}10)$ plane with the close packed basal plane. Geometric description of the stacking and bond structure of the (b) $(20\bar{2})$ zinc blende and (c) $(2\bar{1}10)$ wurtzite planes.	6
Figure 4. Schematic of the $\frac{1}{6}[\bar{1}21]$ partial dislocation before the atoms have relaxed as viewed in the $(20\bar{2})$ plane when (a) a single dangling As bond or (b) three dangling As bonds have been created.	7
Figure 5. Schematic of the (a) 60° $(0002)/\frac{1}{3}[\bar{1}12\bar{0}]$ basal plane, and (b) $[0001]$ threading screw dislocations before the atoms have relaxed to their equilibrium positions.....	8
Figure 6. Schematic of the (a) $(01\bar{1}1)/\frac{1}{3}[\bar{1}12\bar{3}]$ dislocation in the $(2\bar{1}10)$ planar view; (b) stacking sequence of the $(1\bar{1}00)$ planes; and (c) $(11\bar{2}2)/\frac{1}{3}[\bar{1}12\bar{3}]$ dislocation in the $(1\bar{1}00)$ planar view of a wurtzite crystal.	9
Figure 7. Equilibrated dislocations in a SL using material layers that have the FCC zinc blende structure.	11
Figure 8. Stacking faults I1 (ABABCBCBCB), I2 (ABABCACAC), and I3 (ABABCABAB) in comparison with bulk stacking.....	12
Figure 9. (a) Model of an edge dislocation dipole with a $\pm\frac{1}{3}[\bar{1}1-20]$ Burgers vectors and (b) a high resolution STEM image of a single dislocation (<i>I6</i>).....	13
Figure 10. Models for a screw and two threading prismatic edge dislocations.	14

List of Tables

Table 1. Formation energies of the SFs in mJ/m^2	13
--	----

1. Objective

The focus of this work is to determine if it is possible to reduce the concentration of threading dislocations in (0001) oriented hetero-epitaxial aluminum gallium nitride ((Al)GaN) films grown on aluminum nitride (AlN), which have the hexagonal wurtzite structure, much like it has been done for hetero-epitaxial silicon-germanium (SiGe) films grown on silicon (Si) (1, 2), which have the cubic zinc blende structure. Most of the dislocations in the SiGe films have been confined to the region near the substrate, leaving the top of the film where devices are fabricated relatively dislocation free. It is generally agreed that device structures that contain fewer defects produce more reliable and efficient devices. Being able to produce higher quality (Al)GaN device structures will lead to making better high power diodes and transistors in electric vehicles, high electronic mobility transistors (HEMTs) used in radar systems, and ultraviolet (UV) optical emitters used to purify water. In this effort, we also determine the electronic properties of the defects to determine which ones will have the most negative effects on device operation.

2. Approach

The similarities between the face centered cubic (FCC) gallium arsenide (GaAs) zinc blende structure and the hexagonal close packed (HCP) gallium nitride (GaN) wurtzite structure are analyzed to determine what the likely slip system will be for dislocations generated by the planar mismatch strain for growth on an (0001) AlN substrate. This slip system will be used to model the forest of dislocations as they propagate through the growing film. The dangling bond structures of the defects before they have relaxed are determined. They are used as the starting point for the calculations used to determine their relaxed equilibrium structure.

To begin developing a long-term capability to model forests of dislocations in semiconductor and electronic materials, we ported the Parallel Dislocation Simulator (ParaDIS) code (3) originally used to model dislocation motion and generation in FCC metals to the U.S. Army Research Laboratory (ARL) Department of Defense (DoD) Supercomputing Resource Center (DSRC) computers to test the applicability of the code to covalently bound zinc blende FCC bound semiconductors. We employed the code to study the primary mechanisms by which superlattices block threading dislocations (TDs) from reaching the surface. After verifying its applicability to FCC zinc blende structures, our intention is to modify the code so it can be applied to HCP wurtzite semiconductors. This requires knowing what the equilibrium structures of the defects are.

To determine the equilibrium relaxed structures of the defects, we used the density functional method based on total-energy calculations carried out using the Vienna Ab-Initio Simulation Package (VASP) code (4, 5) with projector augmented waves (generalized gradient approximation [GGA]), and defects were introduced into a 60–192 atom wurtzite unit cell of GaN and AlN. Atom positions were relaxed until the forces were less than 0.01 eV/Å with 4–8 k-points; the energy of cut-off was 800 eV. We developed models of the formation of stacking faults (SF) and dislocations in GaN and AlN in order to understand the factors affecting the concentration of the defects created during the growth of both abrupt GaN with and without superlattices, and also with graded AlGaIn structures. We also modeled the elastic and electronic properties of these defects.

3. Results

3.1 Slip Systems Analysis

The nearest neighbor bond structure for GaAs and GaN are identical sp^3 bonds, and the bond structure in the close packed planes is also the same. These planes are the (111) planes in FCC structures and the (0002) planes in HCP structures, and they are crystallographically equivalent. How these close packed planes are stacked on top of each other, however, is different. For GaAs the stacking structure is $A\alpha B\beta C\gamma A\alpha\dots$, while for GaN it is $A\alpha B\beta A\alpha\dots$. The Latin letters represent the stacking of the cations, and the Greek letters represent the stacking of the anions. The α , β , and γ anions lie directly above their corresponding A, B, and C cations. The B-cations lie above one set of interstices in the A-plane defined by three adjacent atoms, and the C-cations lie above the other set of interstices. Four indices instead of three are used to describe the hexagonal crystal structures so that crystallographically equivalent planes are described by similar sets of indices. The redundant additional indice $i = -(h + k)$ is the intercept of the vector $\mathbf{a}_3 = -(\mathbf{a}_1 + \mathbf{a}_2)$, where \mathbf{a}_1 and \mathbf{a}_2 are the hexagonal unit cell vectors in the basal plane. Mismatch dislocations are created by dislocation loops forming at the growing surface and then migrating toward the interface to accommodate the mismatch strain. In the FCC zinc blende structure the primary slip systems are the $\{111\}/\frac{1}{2}\langle 01\bar{1} \rangle$ systems, where the close packed $\{111\}$ planes are the slip planes, \mathbf{S} , on which the dislocations with an edge component move, and the close packed $\frac{1}{2}\langle 01\bar{1} \rangle$ directions are the Burgers vectors, \mathbf{b} , which lie in the slip plane and is the jump distance for the slip. The dislocation line, \mathbf{l} , is the other parameter used to describe a dislocation, and it separates the slipped region from the region where slip has not yet occurred. In the zinc blende structure this is usually the $\langle 10\bar{1} \rangle$ directions. Because \mathbf{b} and \mathbf{l} make an angle of 60° , these dislocations are often referred to as 60° dislocations.

It has been suggested that when indium gallium arsenide (InGaAs) is grown on a GaAs substrate, a dislocation loop composed of a 60° $(111)/\frac{1}{2}[01\bar{1}]$ and a $\frac{1}{2}[01\bar{1}]$ screw dislocation (A screw dislocation is a dislocation in which \mathbf{b} and \mathbf{l} are parallel and there is no \mathbf{S}) nucleates on the

growing surface and moves towards the interface to relieve the strain (6). When the dislocation loop reaches the interface, a 60° $(111)/\frac{1}{2}[01\bar{1}]$ mismatch dislocation with $l = [1\bar{1}0]$ is formed. This is illustrated in figure 1a and b. In the ideal case, the mismatch dislocation will grow and the original dislocation will move out towards the edge thereby greatly reducing the relative lengths of the threading dislocations. This will occur if the dislocation does not get pinned by other dislocations or other defects.

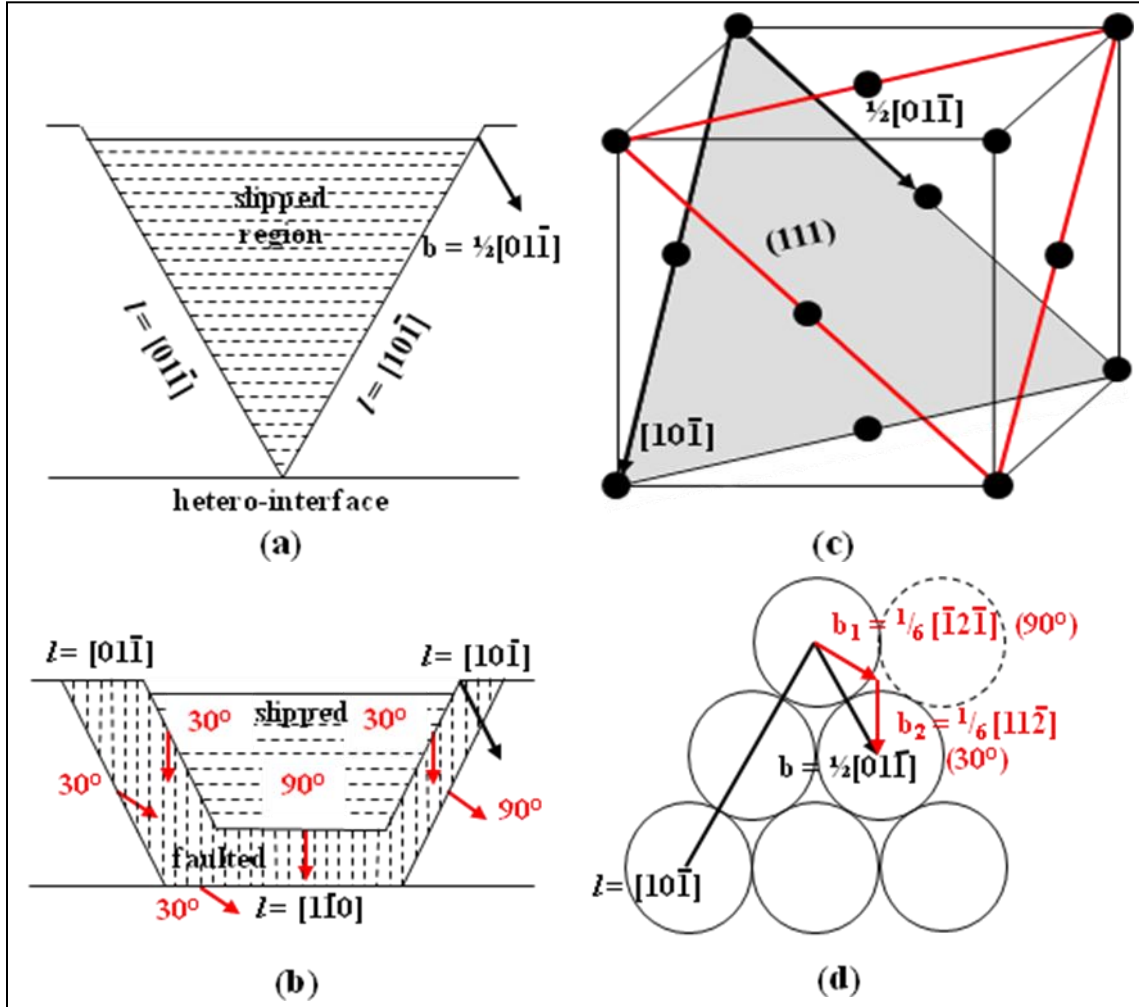


Figure 1. (a) Schematic of a dislocation loop composed of a 60° $(111)/\frac{1}{2}[01\bar{1}]$ and a $\frac{1}{2}[01\bar{1}]$ screw dislocation created at the surface to relieve the mismatch strain. (b) Formation of a third 60° $(111)/\frac{1}{2}[01\bar{1}]$ mismatch dislocation, and all of the associated partials. (c) Schematic of a 60° $(111)/\frac{1}{2}[01\bar{1}]$ dislocation and (d) its decomposition into $\frac{1}{6}[11\bar{2}]$ and $\frac{1}{6}[\bar{1}2\bar{1}]$ partial dislocations.

The dislocation can decompose into two partial dislocations, and this is illustrated in figure 1c and d for the FCC lattice. In this example the $\frac{1}{2}[01\bar{1}]$ dislocation decomposes into $\frac{1}{6}[\bar{1}2\bar{1}]$ and $\frac{1}{6}[11\bar{2}]$ partial dislocations. The $\frac{1}{6}[\bar{1}2\bar{1}]$ partial is normal to the $[10\bar{1}]$ dislocation line and the $\frac{1}{6}[11\bar{2}]$ makes an angle of 30° to it, so they are sometimes referred to as the 90° and 30° partials. The driving force for this to occur is that the energy of a dislocation is $\propto b^2$, and the energy of the two partials, $k(\frac{2}{9} + \frac{2}{9}) < \text{the energy of the single dislocation, } \frac{1}{2}k$. The Burgers vector for the

dislocation is a lattice vector, which means that the atoms in the slip plane are displaced from one stacking position to another identical stacking position. In our example it would be from one B-stacking position to another B-position. However, the displacement associated with a partial dislocation changes the packing sequence. In our example the $\frac{1}{6}[\underline{121}]$ displacement moves the atoms from a B-stacking position to a C-stacking position, and the $\frac{1}{6}[\underline{112}]$ partial displaces atoms in the C-stacking position to the B-stacking position. The new stacking sequence ACABCB... is not the equilibrium stacking sequence, so there is a stacking fault surface energy density, γ_s , associated with it. To determine the area occupied by the SF, one must recognize that the partials repel each other with a force $\propto x^{-2}$, where x is the distance between them. Thus, the equilibrium separation distance between the two partials, d , and therefore the width of the SF is the distance at which $\gamma_s d$ equals the repulsion force.

For hexagonal wurtzite crystals the close packed (0002) plane is usually the primary slip plane, and the slip direction is one of the close packed directions, the $\frac{1}{3}[\underline{2110}]$, $\frac{1}{3}[\underline{1210}]$, and $\frac{1}{3}[\underline{1120}]$ directions (the $[100]$, $[010]$, and $[110]$ in the three indices system). SFs can also be similar. The $60^\circ \frac{1}{3}[\underline{1120}]$ dislocation can decompose into $\frac{1}{3}[\underline{0110}]$ and $\frac{1}{3}[\underline{1010}]$ partials. If the slip plane had B-stacking, the $\frac{1}{3}[\underline{0110}]$ displacement would convert it to C-stacking so the stacking sequence would change to ACBCB...

A primary difference between the GaN and GaAs structures is that the GaN structure has only one close packed plane, not the four that there are in FCC materials. If growth occurs on the (0002) planes, as it most often does, the plane strain created by the mismatch will generate no shear strain in planes parallel or perpendicular to the growth plane; it is a maximum in planes that make a 45° angle with it. Thus, there are no close packed planes in which a shear stress exists to move the dislocations created to accommodate the mismatch strain. Also, dislocations cannot move in the $\{10\bar{1}0\}/\frac{1}{3}[\underline{1210}]$, $\{10\bar{1}0\}/<[0001]>$, $\{11\bar{2}0\}/\frac{1}{3}<\underline{1210}>$ or $\{11\bar{2}0\}/[0001]>$ secondary slip systems because these planes, often called the prismatic planes, are perpendicular to the growth plane. The question then is, what are the most viable secondary slip systems that can accommodate the plane strain in the (0002) plane? Because the shortest vector that does not make a 0° or 90° angle with the $[0001]$ axis is the $\frac{1}{3}<\underline{1123}>$ vector, it is a likely Burgers vector (7). As shown in figure 2, two possible slip planes are the (0111) and (1122) planes. The former makes an angle of 58.4° with the (0002) plane, and the latter makes an angle of 49.0° with it. To determine which one it is, as well as the bonding structure of the defects before they relax to their equilibrium positions, we will construct the appropriate planar views (figure 2).

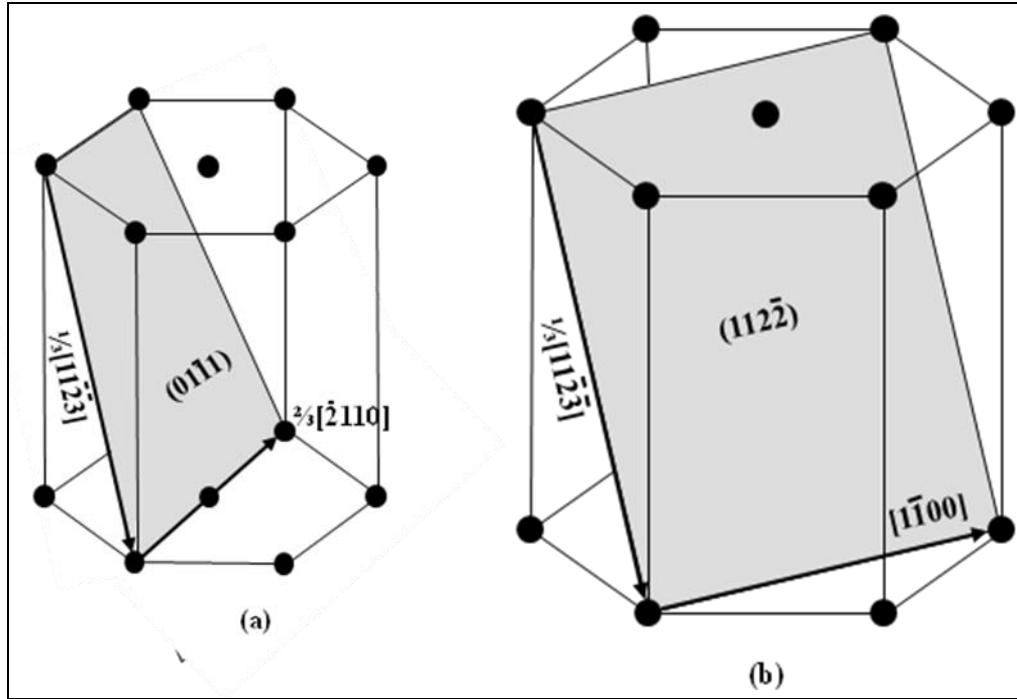


Figure 2. Schematic of the (a) $(01\bar{1})/\frac{1}{3}[11\bar{2}3]$ and (b) $(11\bar{2}\bar{2})/\frac{1}{3}[11\bar{2}3]$ slip systems in hexagonal materials.

The stacking for both the zinc blende and wurtzite crystal structures can be represented by different geometric figures with different colors, and this is shown in figure 3a. The A-cations and α -anions are represented by red circles, the B-cations and β -anions are represented by blue triangles, and the C-cations and γ -anions are represented by green squares. The set of $[\bar{1}21]$ ($[120] \rightarrow [01\bar{1}0]$) traces formed by the intersection of the $(20\bar{2})$ ($(210) \rightarrow (21\bar{1}0)$) planes and the (111) (0002) zinc blende (wurtzite) plane are also shown in figure 3a.

The $(20\bar{2})$ and $(21\bar{1}0)$ planes are perpendicular to the basal plane, the plane of the paper. One can see that these planes have a simple ABA... stacking. As seen in figure 3b and c, these planes contain both cations and anions in equal numbers, which is different from the close packed planes, which contain only one type of atom. Circles are used to describe atoms in the A-plane, triangles are used to represent the atoms in the B-plane behind the A-plane, and squares are used to represent the atoms in the B-plane in front of the A-plane. One can see that two of the four bonds lie in the plane, one points out of the plane, and the fourth points into the plane at the same angle. The larger geometric figure represents a cation, while the smaller represents an anion.

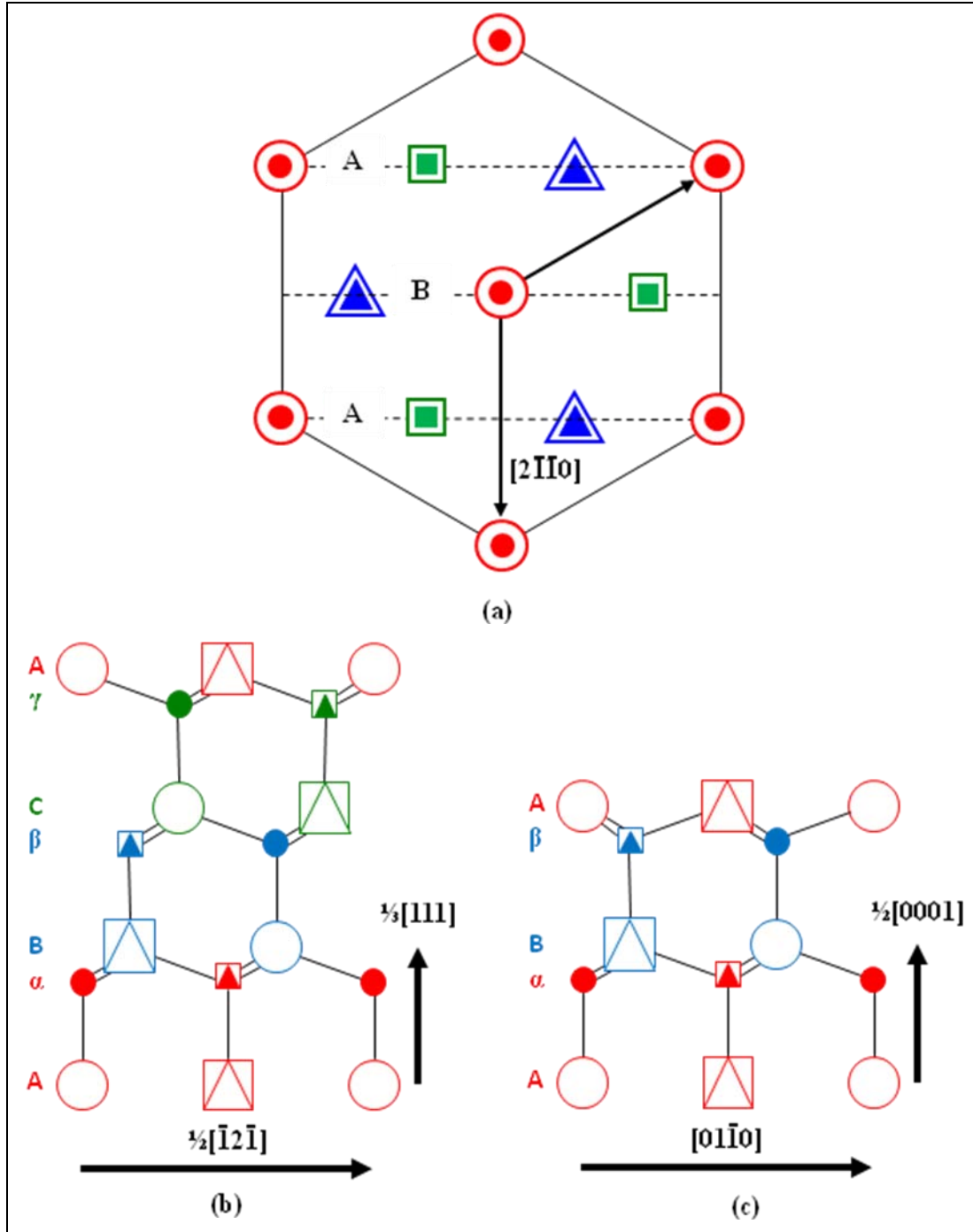


Figure 3. (a) Geometric description of the stacking of the close packed planes in zinc blende and wurtzite crystals, and the $[\bar{1}21]$ or $[01\bar{1}0]$ trace formed by the intersection of the (202) or (2110) plane with the close packed basal plane. Geometric description of the stacking and bond structure of the (b) (202) zinc blende and (c) (2110) wurtzite planes.

The bond structure before the bonds have relaxed, for the stacking fault with the associated $\frac{1}{6}[\bar{1}21]$ partial dislocation in the zinc blende structure discussed earlier is shown in figure 4. (The equivalent partial dislocation in the wurtzite structure is $b_1 = \frac{1}{3}[01\bar{1}0]$.) One can see that a

single or three As (N) dangling bonds could be created depending on where the slip plane lies. (If the “extra half plane” of atoms was above the slip plane instead of below, the dangling bonds would have been Ga [gallium] dangling bonds.) What the stable form is, is determined by the energy of the system.

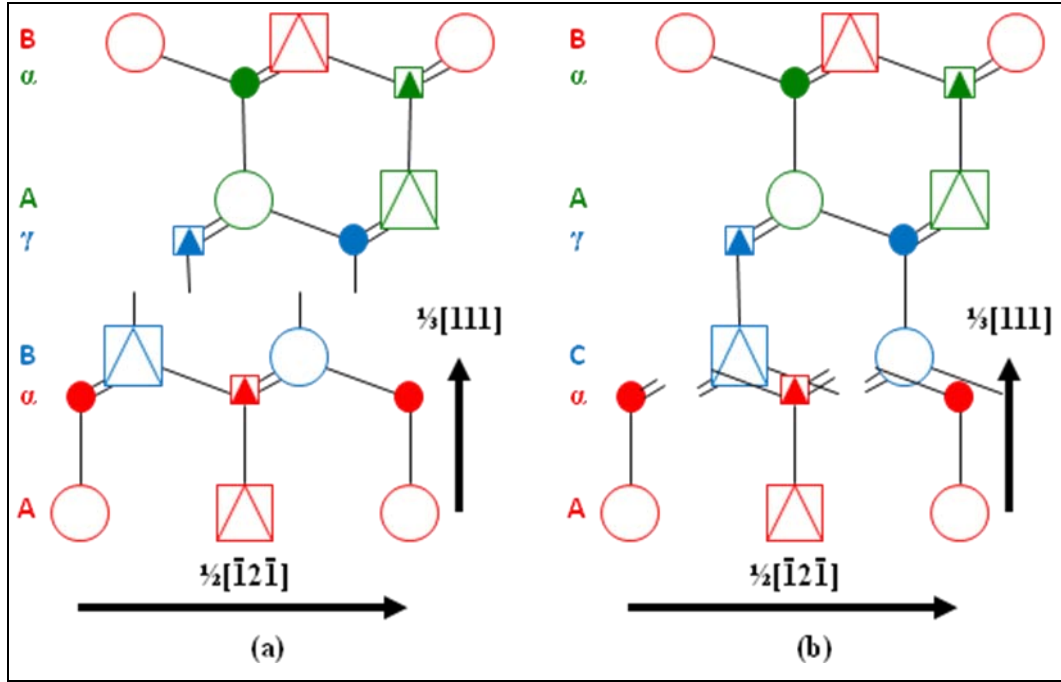


Figure 4. Schematic of the $\frac{1}{6}[\bar{1}2\bar{1}]$ partial dislocation before the atoms have relaxed as viewed in the $(20\bar{2})$ plane when (a) a single dangling As bond or (b) three dangling As bonds have been created.

Having the same (0001) slip plane and $[2\bar{1}10]$ dislocation line as the $\frac{1}{3}[01\bar{1}0]$ partial, the bond structure of the $60^\circ (0002)\frac{1}{3}[11\bar{2}0]$ basal plane dislocation is shown in figure 5a using the same $(2\bar{1}10)$ planar view. The fact that **b** does not lie in the plane of the paper as it does in for the partial does not affect the view of its dangling bond structure. It differs from the 90° partial in that there are dangling bond pairs along the dislocation line instead of a single dangling bond. As indicated by the boxed in area in figure 6a, they can be described as the termination of two extra $(01\bar{1}0)$ half planes at the $[2\bar{1}10]$ dislocation line. Again, the atoms not only will relax to accommodate the strain, now bonds will be made along the dislocation line. How this will be done can be determined by the discrete Fourier transform (DFT) calculations.

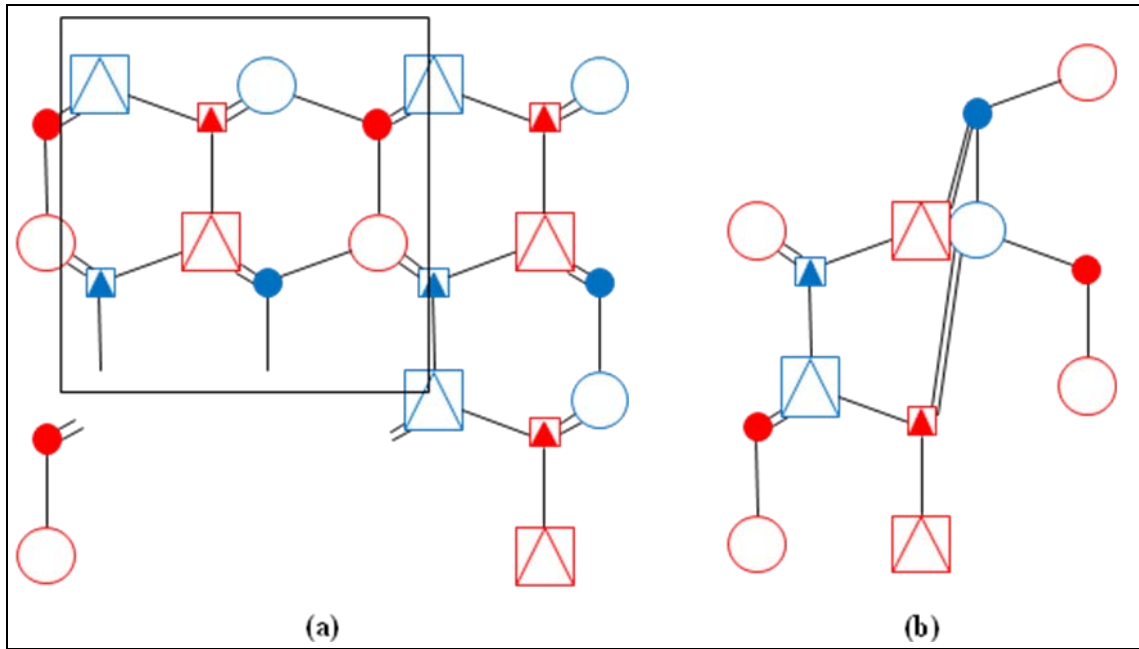


Figure 5. Schematic of the (a) 60° $(0002)/\frac{1}{3}[11\bar{2}0]$ basal plane, and (b) $[0001]$ threading screw dislocations before the atoms have relaxed to their equilibrium positions.

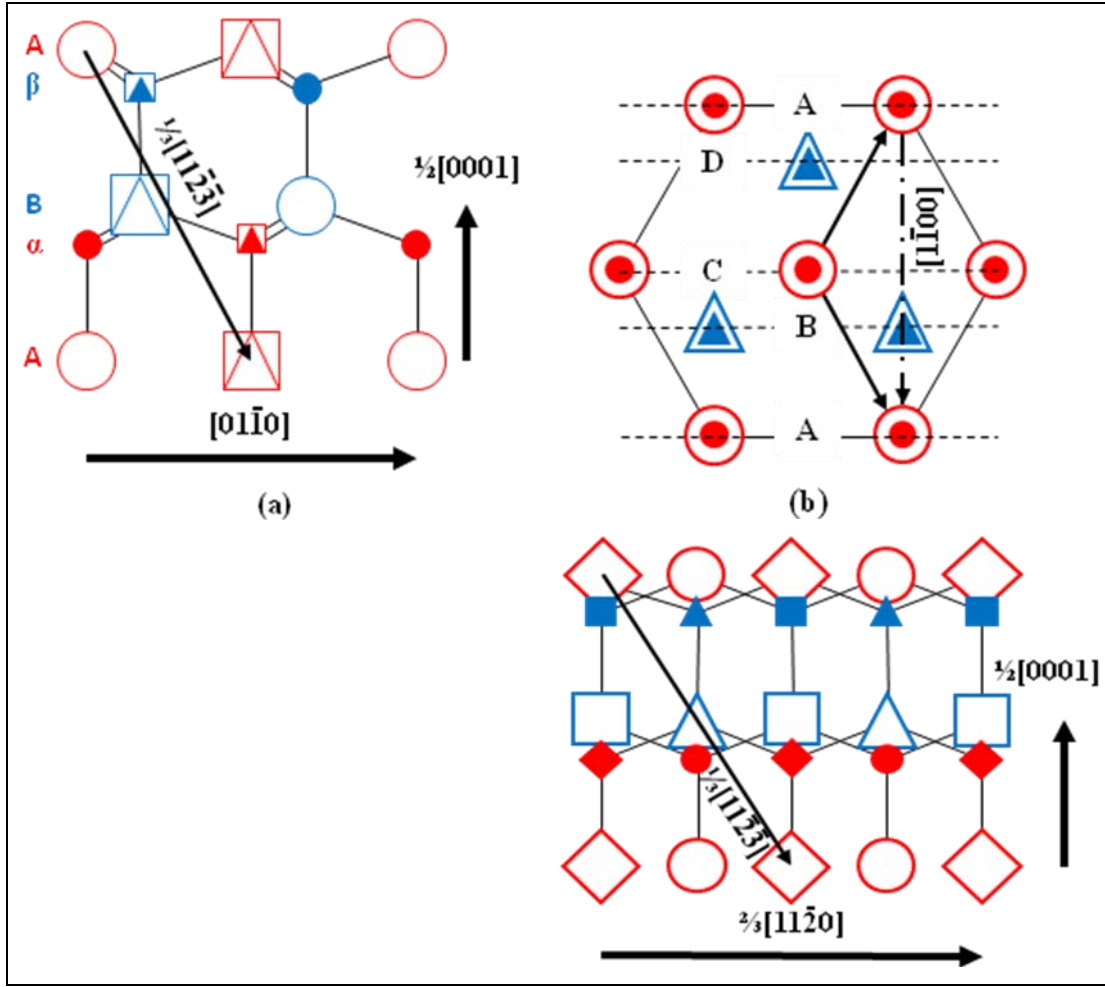


Figure 6. Schematic of the (a) $(01\bar{1}0)\frac{1}{3}[11\bar{2}3]$ dislocation in the $(2\bar{1}10)$ planar view; (b) stacking sequence of the $(1\bar{1}00)$ planes; and (c) $(11\bar{2}2)\frac{1}{3}[11\bar{2}3]$ dislocation in the $(1\bar{1}00)$ planar view of a wurtzite crystal.

The threading edge dislocation, $(01\bar{1}0)\frac{1}{3}[11\bar{2}0]$, has the same \mathbf{b} , but now the dislocation line is parallel to the c -axis instead of being perpendicular to it. The dislocation is said to be an edge dislocation because $\mathbf{b} \perp \mathbf{l}$. If one constructed the stick figure using the (0001) planar view, the plane normal to the dislocation line, one would see that there would be a pairs of dangling bonds along the dislocation line, but instead of being one type of bond, they would be alternating Ga and N bonds. Again the structure can be described by the insertion of two $(01\bar{1}0)$ extra half planes, but this time they terminate along a line parallel to the c -axis. How the bonds are remade and what the equilibrium positions are of the relaxed atoms can be determined by DFT calculations.

Screw dislocations are defined by $\mathbf{b} \parallel \mathbf{l}$. They differ from edge dislocations in that they can be formed by straining bonds instead of breaking them. This is illustrated in figure 5b where there is a schematic of the $[0001]$ threading screw. (Note that a screw dislocation does not have a designated glide plane and associated dangling bonds.) The bonds are so severely stretched that

sometimes hollow core dislocations are formed where creating an internal surface to lessen the high strain energy of these very strong bonds is more energy efficient. Again, DFT calculations can tell us what the stable structure will be.

We now turn to the $\mathbf{b} = \frac{1}{3}\langle 11\bar{2}3 \rangle$ dislocation and the possible (01 $\bar{1}$ 1) and (11 $\bar{2}$ 2) slip planes. If we assume that the dislocation is edge type and most people do, then the dislocation lines are, respectively, the [1 $\bar{1}$ 00] and [2 $\bar{1}$ 10] directions. The (01 $\bar{1}$ 1)/ $\frac{1}{3}$ [11 $\bar{2}$ 3] dislocation is illustrated in the (2 $\bar{1}$ 10) planar view in figure 6a. It can be seen that if this long dislocation were to break up into partials that terminated on the (0002) plane instead of extending all the way to the plane passing through the origin, they would not lie in the (01 $\bar{1}$ 1) plane. The partial dislocations are $\mathbf{b}_1 = \frac{1}{6}[42\bar{3}] \rightarrow [\frac{1}{3} 0 \frac{1}{3} \frac{1}{2}]$ and $\mathbf{b}_2 = \frac{1}{6}[24\bar{3}] \rightarrow [0 \frac{1}{3} \frac{1}{3} \frac{1}{2}]$. Their mutual slip plane is their cross product, $\mathbf{b}_1 \times \mathbf{b}_2 = (112) \rightarrow (11\bar{2}2)$.

To verify with the stick figures that the partials do lie in the (11 $\bar{2}$ 2) plane, and therefore, it is the likely secondary slip plane for the [11 $\bar{2}$ 3] dislocation, one first must determine the stacking sequence for the (1 $\bar{1}$ 00) planes, the planes normal to the [2 $\bar{1}$ 10] dislocation line. As one can see in figure 6b, there are four (1 $\bar{1}$ 00) planes in the repeat distance. Atoms in the A-plane are represented by circles, those in the B-plane by triangles, those in the C-plane by diamonds, and squares represent the atoms in the D-plane. The (1 $\bar{1}$ 00) planar view can be constructed from this (0002) planar view, and it is shown in figure 6c. There it is seen that the two partial dislocations lie in the (11 $\bar{2}$ 2) plane making it more likely that this is the active slip plane for dislocations formed during the growth of (0001) (Al)Ga_{0.5}N on AlN.

This, in fact, is what Srinivasan et al. (8) observed in their transmission electron microscope (TEM) studies of the growth of InGa_{0.5}N on GaN, which is similar to the growth of AlGa_{0.5}N on AlN because the film will be in compression. They concluded that pyramidal slip occurs when epitaxial lateral overgrowth (ELOG) GaN substrates are used because they do not contain large numbers of threading dislocations where pyramidal pits can form to relieve the mismatch strain. They also concluded that the slip plane must be the (11 $\bar{2}$ 2) plane because the dislocation lines they observed were parallel to the [1 $\bar{1}$ 00] direction, and they observed pyramidal dislocations, which most likely were dislocations with a $\frac{1}{3}$ [11 $\bar{2}$ 3] Burgers vector. However, they did not give a physical reason why this occurred. Floro et al. (9) made similar observations in their TEM studies of the growth of AlGa_{0.5}N on GaN even though the films were in tension. They also observed pyramidal slip in addition to the tension induced cracks, as well as what they believed to be partial dislocations, but they mistakenly believed that the $\frac{1}{6}$ [20 $\bar{2}$ 3] and $\frac{1}{6}$ [02 $\bar{2}$ 3] partial dislocations do not lie in the (11 $\bar{2}$ 2) plane.

3.2 Simulations of Dislocation Motion

ParaDIS is a code for doing dislocation dynamics simulations and was specifically written to perform well on massively parallel computers. In it, one introduces dislocation lines into the computational volume and lets them interact and move in response to the forces imposed by external stress and inter-dislocation interactions. To determine how well the ParaDIS code

works for covalently bound zinc blende FCC films grown on a hetero-substrate, we modeled the growth of cadmium zinc telluride (CdZnTe or CZT) on Si using a superlattice (SL) in which the SL layers had different compositions (10). We found that the difference in strain (composition) across layer boundaries plays a key role as to whether a TD might veer away from the interface or continue across it. We also found that while the distance between interfaces has little effect on the motion of a single TD, that it can have an impact of the dislocation tangle as a whole and needs to be considered carefully. We discuss our results in relation to the design of superlattices for TD blocking. The calculations showed that dislocations may penetrate the layers of a SL, and that penetration becomes more likely as the layer thickness decreases. The optimal layer thickness would therefore be just below the critical thickness to avoid the nucleation of new dislocations, while minimizing the ability of dislocations to penetrate through the layer. Figure 7 shows a typical calculation using ParaDIS for strained layer superlattice studies.

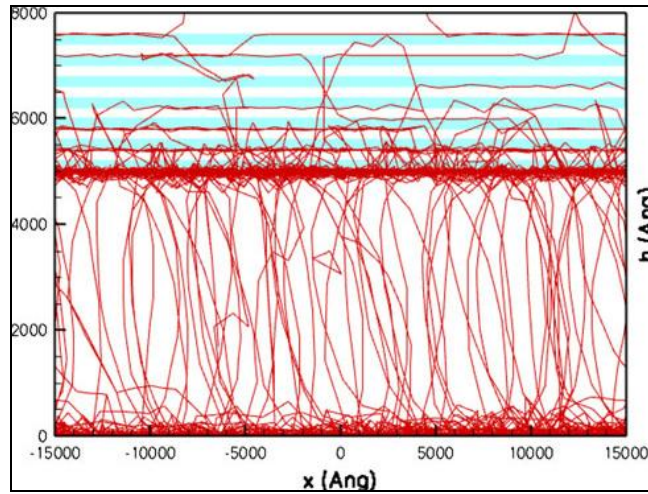


Figure 7. Equilibrated dislocations in a SL using material layers that have the FCC zinc blende structure.

The ability to connect these developments to (Al)GaN systems require considerable new developments and code testing activities in the future. The ParaDIS framework enables solutions to the Peach Koehler forces (11) while coupling to equations of elasticity, which themselves must be solved, to handle defect-defect interactions and interactions with surfaces and interfaces due to finite scale effects. As such, the extension to hexagonal or more sophisticated wurtzite crystals can be done through the following key efforts: (1) identify and implement all slip planes (2) modify ParaDIS to handle 4-Miller indices for hexagonal systems (data structures, variables, etc.), (3) develop and implement dislocation mobility laws relevant for (Al)GaN, and (4) develop and implement appropriate dislocation collision rules.

In addition, ParaDIS requires two fundamental systemic changes. First, it is presently based on Green's Function and boundary element approaches for solving the underlying equations of elasticity. To treat general surfaces and interfaces, the code must be substantially modified to allow arbitrary geometries. For this, a finite element code must be implemented, integrated into the existing ParaDIS framework, and tested. Secondly, the dislocations may not be mobile at room temperature in (Al)GaN. It is therefore important to understand their motion during steps in synthesis and fabrication and include dislocation nucleation during growth and mobility under annealing. We have developed an untested algorithm for layer-by-layer growth within the ParaDIS framework to study the role of changing elastic stresses during film growth at elevated temperature on the dislocation structure.

3.3 Modeling the Defects

Basal stacking faults are quite common defects in GaN and AlN. The main types of relaxed stacking faults that exist in hexagonal wurtzite III-V semiconductors are shown in figure 8.

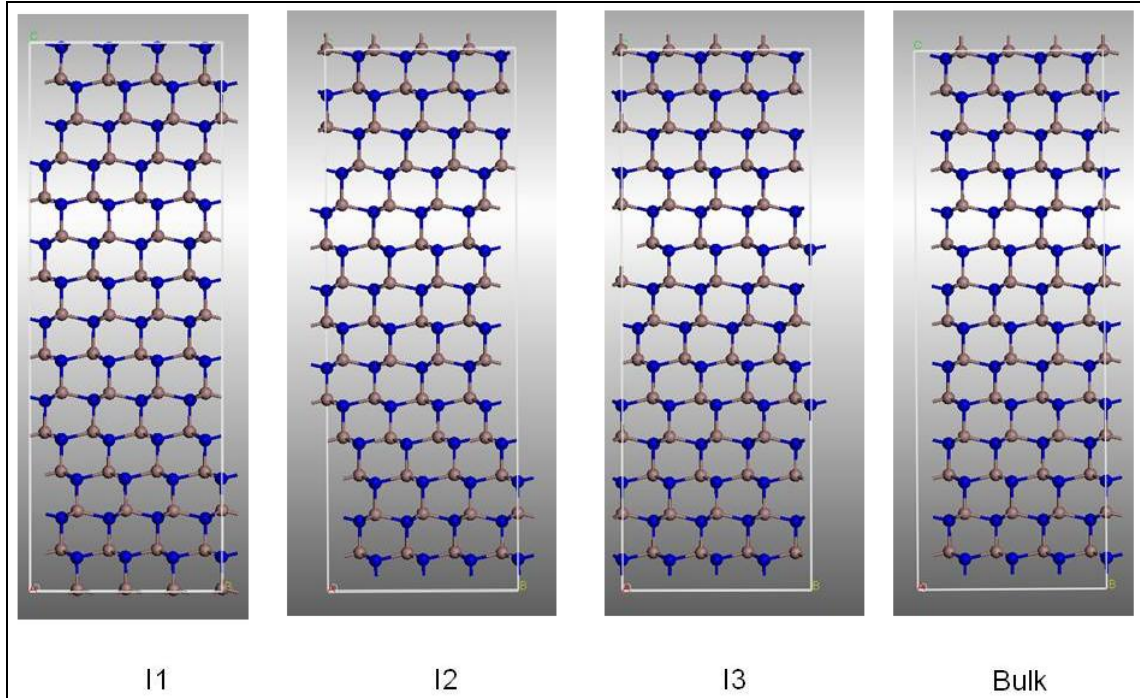


Figure 8. Stacking faults I1 (ABABCBCBCB), I2 (ABABCACAC), and I3 (ABABCABAB) in comparison with bulk stacking.

The energy of formation of a stacking fault is defined as a difference between faulted and unfaulted structures with the same number of atoms divided by the number of stacking faults. It is 2 in the models of I1 (ABABCBCBCBABAB) and I2 (ABABCACACABAB) stacking faults depicted in figure 8. The formation energies of the SFs in mJ/m^2 are presented in the table 1.

Table 1. Formation energies of the SFs in mJ/m².

System\Type of SF	I 1	I 2	I 3
GaN	22	45	26
AlN	79	158	131

The calculated values of the energy of formation stacking faults can be compared with the experimental energy estimated from the width of 60° dislocations obtained with electron microscopy. There is a qualitative agreement of the values 20 ± 3 for GaN and 220 ± 70 mJ/m² (12) with results of our calculations of SFs with an infinite size. There is much experimental evidence that there are SFs of all types present ~90% related to growth (type I) and ~10% related to thermal/strain treatments (type II) in metal organic chemical vapor deposition (MOCVD)-grown GaN (13). Our measurements and simulations support this presence of both types of SFs (14). According to our DFT calculations, strained bonds at the boundary of the finite SF and partial dislocation produce deep filled levels in the band gap of GaN and may be responsible for trapping of the holes.

The threading edge dislocations are the most common dislocation in MOCVD-grown GaN. The concentration of the threading dislocations is $\sim 10^9 - 10^{10}$ cm⁻² of which 68% are pure edge, 30% are mixed, and 2% are pure screw dislocations according to TEM measurements (15). We modeled the dislocation from first principles (figure 9a) and the relaxed structure has a good agreement with the TEM image (figure 9b). We found a set of shallow levels, but no deep levels in the band, which indicates that the edge dislocations are not good candidates for traps of electrons and holes, but could be considered as possible channels for leakage currents. However, the properties trapping properties of the edge dislocation could be changed if dopants and other point defects segregate to the dislocation core.

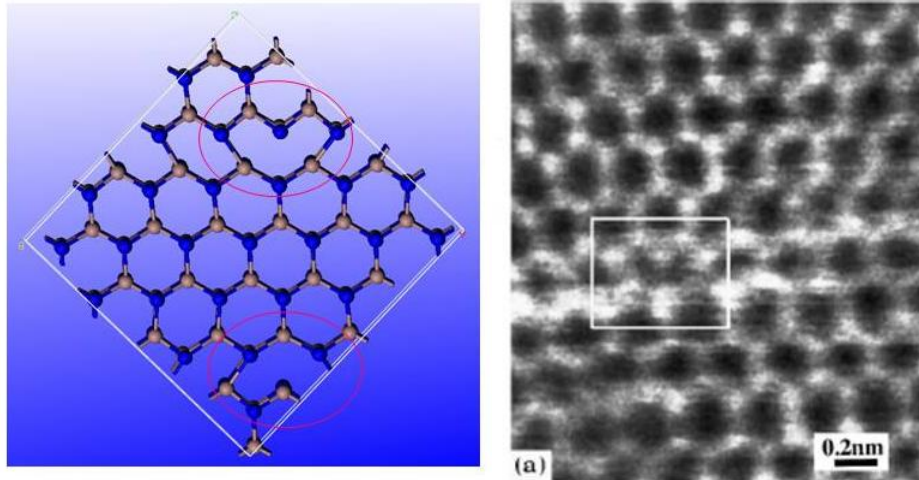


Figure 9. (a) Model of an edge dislocation dipole with a $\pm \frac{1}{3}[11-20]$ Burgers vectors and (b) a high resolution STEM image of a single dislocation (16).

Calculations of the dislocations showed many shallow, but no deep levels in the band gap, which may be related with the fact that the inner surface of the dislocations is similar to the (10 $\bar{1}$ 0) surface of GaN (16). The occupied inner surface states of the dislocations lie just below the valence-band maximum and the empty Ga-derived states lie above the conduction-band minimum. Figure 10 shows models for a screw and two threading prismatic edge dislocations.

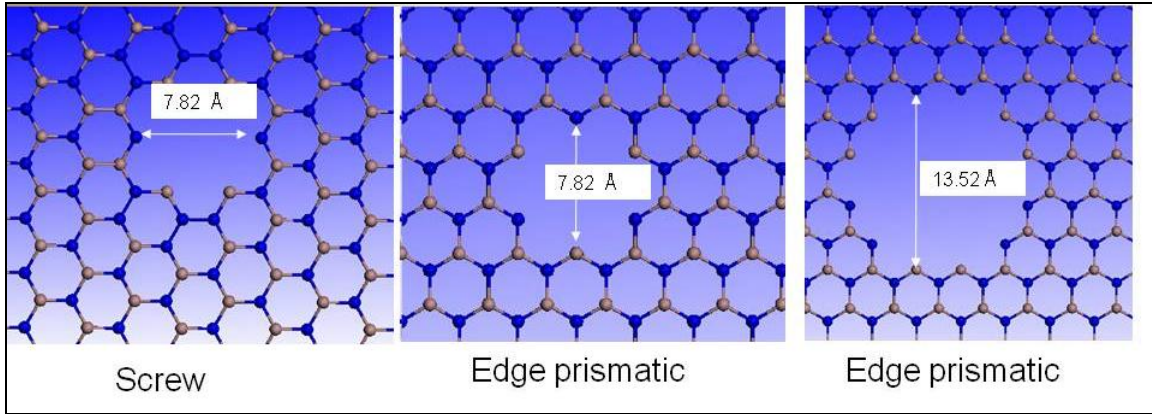


Figure 10. Models for a screw and two threading prismatic edge dislocations.

4. Conclusions

We have done a crystallographic analysis of possible slip systems that could accommodate the mismatch strain for the growth of (Al)GaN films on a (0001) oriented AlN substrate, and have concluded that the most probable one is the $\{11\bar{2}2\}/\frac{1}{3}\langle 11\bar{2}3 \rangle$ system. It contains the shortest dislocation upon which a shear stress created by the plane strain produced by the growth process can act, and it can decompose into $\frac{1}{6}\langle 20\bar{2}3 \rangle$ and $\frac{1}{6}\langle 02\bar{2}3 \rangle$ partial dislocations that lie in the slip plane. Models were also constructed for the bond structure of 60° basal, threading edge, and threading screw dislocations, and some of their associated stacking faults before the atoms have relaxed to their equilibrium positions. They were used to calculate their equilibrium structures and the surface energy of the SFs associated with the partials using density functional theory. The electronic properties of these defects were also calculated, and it was shown that the energy states associated with the dislocations were near or in the conduction or valence bands. However, the partial dislocations appear to create a deep donor about 0.35 eV above the valence band that could act as a hole trap.

In parallel with these efforts we modified the ParaDIS code developed to model the motion of dislocations in FCC metals to model dislocation motion in the covalently bound zinc blende FCC structure, and used it to model the growth of CZT on Si using CZT SL layers of varying compositions. The calculations showed that dislocations may penetrate the layers of a SL, and

that penetration becomes more likely as the layer thickness decreases. The optimal layer thickness would therefore be just below the critical thickness to avoid the nucleation of new dislocations, while minimizing the ability of dislocations to penetrate through the layer.

Our future plans are to develop a more detailed model of the $(11\bar{2}2)/\frac{1}{3}[11\bar{2}3]$ dislocation and the associated $\frac{1}{6}[20\bar{2}3]$ and $\frac{1}{6}[02\bar{2}3]$ partials, and calculate their equilibrium structures and the surface energy of the associated stacking faults, as well as their electronic properties. We will then investigate the possibility that this information can be used to calculate dislocation velocities. This information will be used in an upgraded ParaDIS model that can be applied to semiconductors with the hexagonal close packed wurtzite structure. We will also attempt to verify our modeling efforts using TEM.

5. References

1. LeGoues, F. K.; Meyerson, B. S.; Morar, J. F. *Phys. Rev. Lett.* **1991**, 66, 2903.
2. Meyerson, B. S.; Uram, K. J.; LeGoues, F. K. *Appl. Phys. Lett.* **1988**, 53, 2555.
3. Arsenlis, A.; Cai, W.; Tang, M.; Rhee, M.; Oppelstrup, T.; Hommes, G.; Pierce, T. G.; Bulatov, V. V. *Modeling Simul. Mater. Sci. Eng.* **2007**, 15, 553.
4. Kresse, G.; Hafner, J. *Phys. Rev.* **1993**, B47, 558.
5. Kresse, G.; Furthmuller, J. *Phys Rev.* **1996**, B54, 11169.
6. Nijenhuis, J.; van der Wei, P. J.; van Eck, E.R.H.; Giling, I. J. *J. Phys. D: Appl. Phys.* **1996**, 29, 2961.
7. Yoo, M. H.; Morris, J. R.; Ho, K. M.; Agnew, S. R. *Met and Mater. Trans.* **2002**, 33A, 813.
8. Srinivasan, S.; Geng, L.; Liu, R.; Ponce, F. A.; Narukawa, Y.; Tanaka, S. *Appl. Phys. Lett.* **2003**, 83, 5187.
9. Floro, J. A.; Follstaedt, D. M.; Provencio, P.; Hearne, S. J.; Lee, R. R. *J. Appl. Phys.* **2004**, 96, 7087.
10. Ciani, A. J.; Chung, P. W. *J. of Electronic Mater.* **2010**, 39, 1063.
11. Peach, M.; Koehler, J. S. *Phys. Rev.* **1950**, 80, 436.
12. Takeuchi, S.; Suzuki, K. *Phys.Stat. Sol.* **1999**, A171, 99.
13. Moram, M. A.; Johnston, C. F.; Hollander, J. L.; Kappers, M. J.; Humhpreys, C. J. *J. Appl. Phys.* **2009**, 105, 113501.
14. Batyrev, I. G.; Sarney, W. L.; Zheleva, T.; Nguen, C.; Rice, B. M.; Jones, K. A. submitted to *Physica Stat. Solidi*.
15. Xin, Y.; Pennycook, S. J.; Browning, N. D. *Appl. Phys. Lett.* **1998**, 72, 2680.
16. Northrup, J. E.; Neugebauer, J. *Phys. Rev.* **1996**, B53, R10477.

6. Transitions

This report is for a first-year proposal that we would like to continue for a second year, and then transfer it to the Multiscale Modeling of Electronic Materials effort. Prof. Eugene Fitzpatrick from MIT, who is one of the world's recognized experts in the growth of zinc blende heterojunction device structures and who is partly responsible for the huge successes of the lattice mismatched SiGe devices, has expressed an interest in working on the crystallographically similar III-N wurtzite device structures. We hope that his or a similar group will be integrated into the Multiscale Modeling program to help us carry this work forward.

In a parallel effort, we are working with the people at the Lawrence Livermore Labs who developed the ParaDIS model for FCC metals to determine what alterations, if any, to the code must be made to make the code applicable to covalently bound zinc blende semiconductor crystals. We are also planning to work with them to expand the capabilities of the code to include HCP metals and the closely related semiconductor wurtzite structure.

List of Symbols, Abbreviations, and Acronyms

(Al)GaN	aluminum gallium arsenide
AlN	aluminum nitride
ARL	U.S. Army Research Laboratory
CdZnTe or CZT	cadmium zinc telluride
DFT	discrete Fourier transform
DoD	Department of Defense
DSRC	DoD Supercomputing Resource Center
ELOG	epitaxial lateral overgrowth
FCC	face centered cubic
Ga	gallium
GaAs	gallium arsenide
GaN	gallium nitride
GGA	generalized gradient approximation
HCP	hexagonal close packed
HEMTs	high electronic mobility transistors
InGaAs	indium gallium arsenide
MOCVD	metal organic chemical vapor deposition
N	nitrogen
ParaDIS	Parallel Dislocation Simulator
SiGe	silicon-germanium
SF	stacking faults
Si	silicon
SL	superlattice
TDs	threading dislocations

TEM	transmission electron microscope
UV	ultraviolet
VASP	Vienna Ab-Initio Simulation Package

No of.
Copies Organization

1 (PDF ONLY)	ADMNSTR DEFNS TECHL INFO CTR ATTN DTIC OCP 8725 JOHN J KINGMAN RD STE 0944 FT BELVOIR VA 22060-6218
1 HC	US ARMY RSRCH LAB ATTN RDRL CIM G T LANDFRIED BLDG 4600 ABERDEEN PROVING GROUND MD 21005-5066
3 HCS	US ARMY RSRCH LAB ATTN IMNE ALC HRR MAIL & RECORDS MGMT ATTN RDRL CIM L TECHL LIB ATTN RDRL CIM P TECHL PUB ADELPHI MD 20783-1197
1 HC	US ARMY RSRCH LAB ATTN RDRL SED E KENNETH A. JONES ADELPHI MD 20783-1197
3 HCS	US ARMY RSRCH LAB ATTN RDRL CIH C ANTHONY J CIANI PETER W CHUNG ATTN RDRL WMLB ISKANDER BATYREV BLDG 4600 ABERDEEN PROVING GROUND MD 21005-5066

TOTAL: 9 (1 ELEC, 8 HCS)